

# Porous Silicon

Z. Gaburro, N. Dalosso and L. Pavesi

Dipartimento di Fisica, Università di Trento,  
via Sommarive 14, I-38050 Povo (Trento), Italy  
email: gaburro@science.unitn.it

This chapter deals with generalities and definitions of porous silicon (PSi): fabrication techniques, structural properties, chemical properties, electronics properties, electrical properties, optical properties and actual or potential applications of PSi. Optical properties include light transport, photoluminescence and electroluminescence.

## Generalities and definitions

PSi was discovered by Uhlir in 1956 when performing electrochemical etching of silicon. In 1990, Canham showed that certain PSi materials can have large photoluminescence (PL) efficiency at room temperature in the visible: a surprising result, since the PL efficiency of bulk silicon (Si) is very low, due to its indirect energy band gap and short non-radiative lifetime. The reason of this was the partial dissolution of silicon, which causes i) the formation of small silicon nanocrystals in the PSi material; ii) the reduction of the effective refractive index of PSi with respect to silicon, and hence an increased light extraction efficiency from PSi; and iii) the spatial confinement of the excited carriers in small silicon regions where non-radiative recombination centers are mostly absent. In general, PSi is a interconnected network of air holes (pores) in Si. PSi is classified according to the pore diameter, which can vary from a few nanometers to a few microns depending on the formation parameters (Figure 1). According to the general classification of porous materials, three size regimes are defined as in Table 1.

<Figure 1 near here>

The word *nanoporous* is sometimes used for smallest-pore regime to emphasize the nanometric dimension. The volumetric fraction of air of the material is called *porosity* ( $P$ ). The internal surface of PSi per unit volume can be very large, of the order of  $500 \text{ m}^2 / \text{cm}^3$ . The enhanced photoluminescence efficiency of PSi — compared to Si — has motivated research towards other porous semi-

conductors material. For example, highly porous SiC, GaP,  $\text{Si}_{1-x}\text{Ge}_x$ , and Ge structures have been investigated.

## Fabrication procedures

### *Anodization*

PSi is mostly fabricated by electrochemical anodization — often referred to as electrochemical etching — of bulk Si wafers in diluted aqueous or ethanoic hydrofluoric acid (HF). Ethanol is often added to facilitate evacuation of  $\text{H}_2$  bubbles, which develop during the process. Typical anodization arrangements are schematically shown in Figure 2. Another much less common technique is stain etching, or chemical etching (with no current flow), performed with HF- $\text{HNO}_3$  solution.

<Figure 2 near here>

The anodization can be performed either in *potentiostatic* (voltage-controlled) or in *galvanostatic* (current-controlled) mode. The latter is normally preferred, because it supplies the required charge for the reaction at constant rate, regardless of any evolution — during anodization — of the cell electrical impedance, ultimately leading to more homogeneous and reproducible material. The typical values of the most important anodization parameters, along with their impact on the anodization process, are reported in Tables 2 and 3. Three sample setups for fabrication of different PSi structures are shown in Table 4. The anodization can be modulated. The modulation is most easily achieved by varying the applied current density. Modulation results in controlled changes of the microstructure and the porosity of PSi along the growth direction. For example, PSi multilayer films can be simply created by varying the current density in time.

<Figure 3 near here>

The position of pore nucleation can be controlled by *etch pits*, defined by a lithographic step before the anodization (Figure 3). This option is in practice limited to macroporous PSi, since present lithographic resolution lowest limits are in the range of a hundred of nm. For example, ordered two-dimensional periodical matrices of pores can be formed, leading to materials with remarkable optical transport properties (2D photonic crystals, see Figure 4).

PSi single or multi-layers can be fabricated as *free-standing* samples. The detachment from the substrate can be achieved by applying a short pulse of high current density — i.e. exceeding the electropolishing threshold, typically some hundreds mA/cm<sup>2</sup>.

<Figure 4 near here>

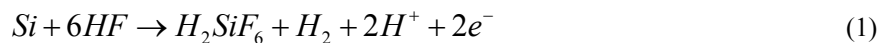
### **Anodization mechanisms**

Typical current-voltage (I-V) characteristics of the electrochemical cell are shown in Figure 5. It should be stressed that the quantity having physical meaning is the current density  $J$  (at the Si/electrolyte interface), rather than the absolute current  $I$ .  $J$  and  $I$  scale with a fixed constant for a given cell, provided that the area of the Si sample exposed to the electrolyte is well defined and fixed.

<Figure 5 near here>

To form PSi, the current at the Si side of the Si/electrolyte interface must be carried by *holes*, injected from the bulk towards the interface. The current must be kept between zero and the electropolishing threshold, which can be identified as the value of the first maximum of the anodic regime in the I-V curve. Useful regimes are included in the hashed region of Figure 5, where the electropolishing threshold voltage (for the curve marked with hollow circles) is  $V \approx 1.3$  V. In order to achieve significant hole current in n-type Si, external illumination of the sample is required, depending on the doping level. If the current exceeds the electropolishing threshold, the anodization results in a progressive, complete removal of Si. The wafer has then a mirror-like appearance.

A hypothesized chemical reaction which could describe the anodization is



The last term — a negative charge at the interface, to be neutralized by the current flow — would explain the need of hole injection from the substrate towards the Si/electrolyte interface.

Similarly to most semiconductor junctions, at the Si/electrolyte interface a depletion zone is formed. The width of this depletion zone depends on the doping and may explain the different pore sizes found in  $p^-$  and  $p^+$  type doped silicon. In addition, the depletion layer width depends on the surface curvature: the anodization preferentially occurs at the pore tips where the curvature is largest. Moreover, when the depletion zones of adjacent pores meet each other, the current flow is suddenly pinched off. Further Si etching is blocked, and pore collapsing is prevented. For this reason the reaction is self limited in the hashed anodization regimes of Figure 5 and leads to a porous structure

rather than to electropolishing. As further practical consequence, in stationary conditions, the porosity remains approximately constant, whereas the overall thickness of the PSi layer grows essentially linearly in time.

Back-side illumination (most conveniently achieved using cells of type B, Figure 2) in potentiostatic regime, with n-type Si, allows an useful, further control on the hole injection, both in terms of carrier flux (which is proportional to illumination intensity) and of localization of the injection, which is concentrated in the region of the pore tips, acting as hole collectors. The etching process leads to a very regular pore growth which is most effectively exploited to fabricate macroporous photonic crystal devices (Figure 4).

### *Drying techniques*

Due to large capillary stress, drying of samples is a critical step and can result in extended cracking if special procedures are not followed. Methods to reduce or eliminate the capillary stress include pentane drying, supercritical drying, freeze drying and slow evaporation rates. Pentane drying is the easiest to implement. Pentane has a very low surface tension, and shows no chemical interaction with PSi (unlike ethanol). Using pentane as drying liquid enables to reduce strongly the capillary tension, but since water and pentane are non-miscible liquids, ethanol or methanol have to be used as intermediate liquids. Using this drying technique PSi layers with porosity values up to 90 % and thickness up to 5  $\mu\text{m}$  exhibit no cracking pattern after drying. Supercritical drying requires a specific apparatus but is more effective in preventing cracking of the film so that PSi layers of porosity values up to 95 % were demonstrated.

### *Oxidation techniques*

As soon as PSi samples are dried, hydrogen surface passivation is gradually replaced by native oxide. This chemical change affects most PSi properties, for example photoluminescence and electrical conductivity. Since the characteristics of the native oxide strongly depend on many factors such as the storage conditions, evolution of sample properties are often poorly characterizable. To stabilize PSi properties oxidation is often used. Oxidation implies the formation of a layer containing the original Si atoms. Therefore, it also reduces the nanocrystallite size, with remarkable impact on photoluminescence emission energy (blue-shift). The employment of controlled oxidation procedures is therefore a valuable post-anodization option towards a better control of PSi properties and stabilization.

Tested oxidation procedures on PSi include anodic oxidation, chemical oxidation, thermal oxida-

tion, plasma assisted oxidation and irradiation enhanced oxidation. Anodic oxidation is an electrochemical process, in which oxide layers are formed with current injection. As such, the technique is structurally selective: more conductive paths gets more oxidized. This selectivity is particularly interesting for light emitting diode (LED) applications, where more conductive paths are usually associated to large injection channels, which are poorly luminescent, and their oxidation results in enhanced electroluminescence quantum efficiency. Another application of controlled oxidation — mostly thermal — is the fabrication of small, blue-luminescent PSi nanocrystallites.

## Structural properties

Structural properties of PSi have been investigated by Electron microscopy, Scanning probe microscopy, X-ray scattering techniques, X-ray absorption techniques, and Raman spectroscopy. In particular, X-ray absorption spectroscopy can be performed not only by extended X-ray absorption fine structure (EXAFS) analysis, but also by X-ray excitation of optical luminescence (XEOL), a convenient tool for luminescent sample, in which absorption is probed via the measurement of the corresponding optical emission. A general feature resulting from the comparison of these techniques is that highly luminescent PSi is a composition of variously connected *Si crystals* of nanometric dimensions (typically, 1 to 5 nm in radius). Smaller sizes than Si Bohr radius ( $\approx 4.9$  nm) imply significant quantum confinement effects. Raman measurements are also often used to demonstrate crystallinity in PSi skeleton and infer information on the size of Si nanocrystals.

Accurate determination of pore size distribution in mesoporous Si is usually given by the analysis of adsorption isotherms of gases at low temperature (Brunauer-Emmett-Teller, or BET, method). The physical adsorption by a porous surface is increased relative to a non-porous one because of capillary condensation in pores. This increase in adsorption starts when the gas pressure is high enough to fill the smallest pores.

## Chemical properties

Surface chemical composition of PSi is best probed with Fourier Transform InfraRed (FTIR) spectroscopy. FTIR signal in PSi is larger and easier to measure than in bulk Si due to much larger specific area. Chemical bonds and their IR resonance positions detected in PSi are shown in Table 5. In fresh, as-prepared samples, oxygen is normally absent, the dominant bonds being Si-H<sub>x</sub> groups ( $x = 1, 2$  or  $3$ ). Ageing is observed as a slow replacement of H by O bonds in PSi. Also luminescence fatigue is explained by photochemical reactions occurring on the surface of the Si nanocrystals.

## Electronic properties

The first and most favorable explanation for the visible emission in PSi is the quantum confinement of excitons in nanometer sized silicon. An empirical law, based on the effective mass approximation, links the energy gap  $E_g$  of silicon nanocrystals with their sizes  $\ell$ :  $E_g(\ell) = E_g^{Si} + 88.34/(\ell)^{1.37}$  (eV), when  $\ell$  is given in Å. The energy gap opening is given by an equal energy shift of the bottom of the conduction band to high energy and of the top of the valence band to low energy. The nature of the energy-gap is still indirect even though a quasi-direct band gap can be formed in ultra small Si nanocrystals.

## Electrical properties

Electrical resistivity in PSi is five orders of magnitude higher than in intrinsic Si, because PSi is depleted by free carriers. Depletion can occur either because of the energy gap widening from quantum confinement which reduces the thermal generation of free carriers, or because of trapping of free carriers. Trapping can occur during the preparation of PSi either because the binding energy of dopant impurities are increased or because of the formation of surface states. It has been demonstrated that the dopants are still present in essentially unchanged concentration after the etching, but are in a neutral state.

The electrical transport is mainly affected by the disordered structure of the Si skeleton which restricts the conductive paths to a highly constrained geometry, which for certain porosities forms a percolated or fractal geometry. As a consequence conductivity is thermally activated, strongly frequency dependent and highly dispersive. Several models have been proposed to explain the electrical transport properties. They differ on the transport paths and mechanisms. The proposed transport paths range from transport in the Si nanocrystals (with diffusion or tunneling between the Si nanocrystals or at their surface), to transport in the amorphous and disordered matrix surrounding the nanocrystals, or through both. The suggested mechanisms are band transport, activated hopping in band tail, trap controlled hopping through nanocrystals, activated deep states hopping, Pool-Frenkle processes and activated hopping in a fractal networks.

Given the large specific area per unit volume, the electrical transport is strongly influenced by external factors such as residual electrolyte and ambient atmosphere. The latter property is very interesting for sensor applications. Certain gases — for example  $\text{NO}_2$  — have the capability of modifying the free carrier population. Changes in the electrical conductivity in presence of sub-ppm concentrations of such gases can be detected at room temperature operation. Other gaseous species (for example polar liquid vapors) also affect electrical transport via electric field interactions with char-

ge carriers.

## Optical properties

### *Light diffusion and scattering*

The dimension  $\ell$  of the PSi structures (i.e., the pore size and the porous layer thickness), compared to the optical wavelengths  $\lambda$ , can range from  $\ell \ll \lambda$  all the way to  $\ell \approx \lambda$ . There are accordingly two different regimes of light propagation and interaction with PSi.

The *first regime* is  $\ell \ll \lambda$ . The radiation fields cannot resolve the PSi structures, and the interaction can be conveniently described by means of an *effective medium approximation*, where a macroscopic dielectric constant (or a refractive index) is evaluated as a suitable combination of the dielectric constants of Si and air. The result is in general a complex dielectric function of space. Effective medium theories, which are routinely used for PSi, are enumerated in Table 6. Refractive index values are reported in Figure 6.

<Figure 6 near here>

The *second regime* is  $\ell \approx \lambda$ . This kind of structures are called *mesoscopic*: the structural size is small compared to the *wave coherence length* — i.e. the maximum length along which phase memory and coherent phenomena are observable. The porous geometrical structure strongly influences light transport and interaction. Useful mathematical models take advantage either of the Bloch theorem, in the case of periodical structures (photonic crystals), or of statistical and Green's function methods, in the case of aperiodic or random structures.

*Mixed regimes* are also possible in PSi. The most important case are one-dimensional (1D) mesoscopic structures: the anodization parameters are set to achieve microporous PSi, (size of pores  $\ll \lambda$ , first regime), but the anodizing current density is modulated to obtain periodical or aperiodical thin layer structures (thickness  $\approx \lambda$ , second regime along the PSi growth direction). Each layer is different from adjacent layers in terms of porosity and thus of effective dielectric constant (and effective refractive index). Compared to other thin-film growth techniques, PSi has the advantage of allowing a *continuous* tuning of the refractive index over a wide range ( $1.4 \leq n_{eff} \leq 2.4$ ), and of being a fast and cheap technique that can lead to structures of several *hundreds* of layers, with typical fabrication times ranging from few minutes to few hours.

In presence of high-index liquids (and/or their vapors), the refractive index of the porous layer

changes, affecting light transport properties. The effect can be exploited for gas sensors and biosensors applications.

## **Photoluminescence**

Microporous PSi structures have been reported to luminesce efficiently in the near infrared (IR) (0.8 eV), in the whole visible range and in the near ultraviolet (UV) (Figure 7).

<Figure 7 near here>

Such a broad range of emission energies arises from a number of clearly distinct luminescent bands, which are listed in Tables 7, 8, and 9. In addition, PSi has been used as an active host for rare earth impurities, e.g. Nd or Er, or dye solutions. Direct energy transfer between PS and the impurity or dye is demonstrated. The most efficient and studied emission is the slow (S) band because it can be excited by electrical injection. The most popular model for the photoluminescence — especially for the S-band — is excitonic radiative recombination subject to quantum confinement. Other models are surface states models, the siloxene model, defect models, the surface hydrides model and the hydrogenated amorphous silicon model. Coexistence of more than one mechanism is likely.

### **S-band**

It can be tuned from close to the bulk silicon band gap through the whole visible range. The large spectral width comes from inhomogeneous broadening and vibronic coupling of the radiative transitions. The S-band efficiency is not proportional to the inner surface area: a “threshold” porosity has to be exceeded to achieve an efficient luminescence. Post-anodization chemical etching in HF, corresponding to a porosity increase, results in a strong rise in PL efficiency and a blue shift of the visible band. External quantum efficiencies higher than 0.1 % are obtainable from high porosity PSi layers of all types, but efficiency normally decreases in the order  $n^-$ -type,  $p^-$ -type,  $n^+$ -type,  $p^+$ -type doped PSi. High porosity is essential for high visible PL efficiency. The inefficient luminescence observed from inhomogeneous material of low porosity originates from microscopic areas of high porosity. Isolated nanocrystals, produced by dispersing a colloidal suspension of PSi fragments on a glass coverslip, show external quantum efficiencies  $\geq 88\%$ , with a number of bright to dark nanocrystals in the suspension of only 2.8 %. Thus, the average quantum efficiency of a PSi layer of 1% results from a statistical distribution of high and low quantum efficiency nanocrystals.

Phonon-assisted luminescence (vibronic coupled transitions) is demonstrated by fine structure in resonantly excited photoluminescence at low temperature. Thus, the electronic and the vibronic

structure of the luminescence of PSi are similar to crystalline Si, with an energy shift consistent with quantum confinement. At large confinement energies ( $> 0.7$  eV), no-phonon quasi-direct transitions dominate, because of breakdown of k-conservation under strong confinement.

The luminescence is polarized parallel to the exciting light. This is measured by recording the polarization ratio  $\rho = (I_{\parallel} - I_{\perp}) / (I_{\parallel} + I_{\perp})$ .  $\rho$  is zero on the IR band and non-zero on the *S*-band (tending to zero as the energy approaches that of the Si band gap). The interpretation is that PSi is an ensemble of randomly oriented aspherical nanocrystals, preferentially aligned along the  $\langle 100 \rangle$  direction. Recombining carriers have bulk-like wavefunctions which are sensible to the shape of the nanocrystals.

Aging effects include a blue-shift in the *S*-band and changes in the photoluminescence efficiency (both increases and decreases have been observed), which can be explained in terms of surface oxidation. Anticorrelation exists between the dangling bond density and the luminescence efficiency, thus the effect of the oxidation depends on its passivation properties.

### **Other bands**

The F-band is observed only in oxidized PSi, and it is probably originated from contaminated or defective Si oxide. Annealing in water vapor activated the blue emission indicating a possible major role of adsorbed hydroxyls in the emission process.

The IR band is weak at room temperature, and becomes much stronger at cryogenic temperatures. Its origin seems to be related to dangling bonds, although no direct correlation has been demonstrated.

### ***Absorption***

The absorption coefficient has been measured in PSi by optical transmission, photoluminescence excitation (PLE), and photothermal deflection spectroscopy (PDL). Transmission spectra are shifted towards higher energy compared to bulk Si with a shift which increases with increasing porosity. This observation is consistent with quantum confinement model.

The lineshape analysis of the absorption coefficient shows that its energy dependence follows a trend like that of an indirect gap semiconductor similar to Si, but displaced to higher energy.

<Figure 8 near here>

A characteristic feature of PSi is the large displacement (Stokes-shift) between the absorption edge and the emission peak energy (see Figure 8). The existence of localized states that can account for

the observed shift has been demonstrated. Such states can lead to self-trapped excitons at some surface bonds of Si crystallites, such as Si-Si dimers and Si-O double bonds, giving reduced dependence of the luminescence energy on size, and a very large Stokes shift. Other models for the Stokes-shift are based on Si quantum dot relaxation from distorted configurations, giving rise to new transitions involving localized states that lower the emission threshold with respect to the absorption.

## Applications

Main actual or perspective applications of PSi are shown in Table 10.

### *Light emitting diodes (LEDs)*

Si p/n junction emit light both in forward and in reverse bias conditions. Power efficiency is about  $10^{-4}$  ( $10^{-8}$ ) at 1.1  $\mu\text{m}$  wavelength in forward (reverse) bias. Also in PSi based devices, electroluminescence (EL) is observed both in the IR and in the visible. Efficiency is higher than in bulk Si diodes, depending on the diode structure and on the PSi contact method. Initially observed with wet contacts, EL was then reported with solid contacts. Major achievements in terms of quantum efficiency are summarized in Figure 9.

<Figure 9 near here>

### *Sensors, biosensors, medical applications*

PSi is a two-fold promising material for sensor applications. On one side, its electrical and optical properties strongly depend on the environment, because of its large specific area. Useful sensing parameters include, for example, the electrical conductivity and photoluminescence. Most sensing parameters can effectively work at room temperature. On the other side, it supplies a handy template to hold chemical and biological species. Target species can be immobilized in the PSi matrix, a practice which is especially useful for biological samples — such as oligonucleotides, biotin or antibodies. Techniques for immobilization range from physical adsorption to the replacement of hydride bonds with Si alkyls, and to antibody bonding at functionalized PSi surface with subsequent antibody-antigen interactions. Species identification can be performed by probing optical, electrical or chemical properties. Examples include, respectively, reflectivity or waveguiding measurements (which depend on the dielectric constant of the species, as already discussed), conductance measurements, and pH measurements. Biocompatibility of PSi has suggested medical applications, such as in vivo slow release of drugs, in vivo diagnostic tests, and template for bone growth.

## Bibliography

- Canham LT (1990), Silicon quantum wire fabrication by electrochemical and chemical dissolution of wafers, *Appl. Phys. Lett.* 57 (10), 1046–1048.
- Smith RL, Collins SD (1992), Porous silicon formation mechanisms, *J. Appl. Phys.* 71 (8), R1–R22.
- Gösele U, Lehmann V (1995), Light-emitting Porous Silicon, *Mater. Chem. Phys.* 40 (4), 253–259.
- Brus L (1996), Semiconductor colloids: Individual nanocrystals, opals and porous silicon, *Curr. Opin. Colloid. In.* 1 (2) 197–201.
- Amato G, Delerue C, von Bardeleben HJ (eds.) (1997) Optical and Structural Properties of Porous Silicon Nanostructures, in Manasreh M. O. (series ed.), *Opto-Electronic Properties of Semiconductors and Superlattices*, Vol. 5, Gordon and Breach, Newark, 1997.
- Cullis AG, Canham LT, Calcott PDJ (1997), The structural and luminescence properties of porous silicon, *J. Appl. Phys.* 82 (3), 909–965.
- Sailor MJ, Heinrich JL, Lauerhaas JM (1997), Luminescent porous silicon: Synthesis, chemistry, and applications, *Stud. Surf. Sci. Catal.* 103, 209–235.
- Yerokhov VY, Melnyk II (1999), Porous silicon in solar cell structures: a review of achievements and modern directions of further use, *Renew. Sust. Eberg. Rev.* 3 (4), 291–322.
- Bisi O, Ossicini S, Pavesi L (2000), Porous silicon: a quantum sponge structure for silicon based optoelectronics, *Surf. Sci. Rep.* 38 (1-3), 5–126.
- Stewart MP, Buriak JM (2000), Chemical and biological applications of porous silicon technology, *Adv. Mater.* 12 (12), 859–869.
- Föll H, Christophersen M, Carstensen J, et al. (2002), Formation and application of porous silicon, *Mat. Sci, Eng. R* 39 (4), 93–141.
- Buriak JM (2002), Organometallic Chemistry on Silicon and Germanium Surfaces, *Chem Rev.* 102 (5), 1272–1308.
- Gelloz B, Koshida N (2003) Electroluminescence of Nanocrystalline Porous Silicon Devices, in *Handbook of Luminescence, Display Materials, and Devices*, Edited by H. S. Nalwa and L. S. Rohwer, Chapter 5, 127–156.
- Filler MA, Bent SF (2003), The surface as molecular reagent: organic chemistry at the semiconductor interface, *Progress in Surface Science* 73, 1–56.
- Ossicini S, Pavesi L, Priolo F (2003), Light Emitting Silicon for Microphotonics, *Springer Tracts in Modern Physics* vol. 194 (Springer-Verlag, Berlin 2003).

## Tables

Table 1. IUPAC classification of porous materials

Dominant pore width (nm)	Type of material
$\leq 2$	microporous
2-50	mesoporous
$> 50$	macroporous

Table 2. Critical parameters of the anodization procedure. A typical electrochemical solution can include, for example, water (H<sub>2</sub>O) in approximately equal amount of HF, the rest being ethanol.

Parameter	Typical range	Unit
HF concentration	2 - 40	% (in weight)
Current density	0.5 - 150	mA/cm <sup>2</sup>
Anodization time	5 - 1800	s
Temperature	250 - 300	K
Wafer resistivity ( <i>p</i> -type)	0.001 - 100	Ω cm
Wafer resistivity ( <i>n</i> -type)	0.001 - 100	Ω cm

Table 3. Effect of anodization parameters on PSi formation. As an approximate rule of thumb, the etch rate is of the order of 1 nm/s for each mA/cm<sup>2</sup> of the anodization current density.

An increase of	results in a		
	Porosity	Etching rate	Electropolishing threshold
HF concentration	decrease	decrease	increase
Current density	increase	increase	-
Anodization time	increase	almost constant	-
Temperature	-	-	increase
Wafer doping ( <i>p</i> -type)	decrease	increase	increase
Wafer doping ( <i>n</i> -type)	increase	increase	-

Table 4. Three *sample* sets of anodization parameters, for p-type Si substrates, resulting in the three different structural regimes described in Table 1.

HF concentration (%)	15	15	2
Current density (mA/cm <sup>2</sup> )	50	50	5
Wafer resistivity ( $\Omega$ cm)	5	0.01	10
Resulting structure	Microporous	Mesoporous	Macroporous

Table 5. Wavenumber positions and attributions of the absorption peaks observed in several p-Si samples by Fourier transform infrared absorption FTIR measurements.

Peak position ( $\text{cm}^{-1}$ )	Attribution	Peak position ( $\text{cm}^{-1}$ )	Attribution
3610	OH stretch. (SiOH)	1463	$\text{CH}_3$ asymmetric deformed
3452	OH stretch. ( $\text{H}_2\text{O}$ )	1230	$\text{SiCH}_3$ bending
2958	CH stretch. ( $\text{CH}_3$ )	1056-1160	SiO stretching in
2927	CH stretch. ( $\text{CH}_2$ )		O-SiO and C-SiO
2856	CH stretch. (CH)	979	SiH bend. in $\text{Si}_2\text{-H-SiH}$
2248	SiH stretch. ( $\text{O}_3\text{-SiH}$ )	948	SiH bend. in $\text{Si}_2\text{-H-SiH}$
2197	SiH stretch. ( $\text{SiO}_2\text{-SiH}$ )	906	$\text{SiH}_2$ scissor
2136	SiH stretch. ( $\text{Si}_2\text{O-SiH}$ )	856	$\text{SiH}_2$ wagging
2116	SiH stretch. ( $\text{Si}_2\text{H-SiH}$ )	827	SiO bend. in O-Si-O
2087	SiH stretch. ( $\text{Si}_3\text{-SiH}$ )	661	SiH wagging
1720	CO	624	SiH bending in ( $\text{Si}_3\text{SiH}$ )

Table 6. Useful effective medium approximation for the dielectric function of PSi. The symbols have the following meanings:  $\varepsilon$ , Dielectric function of Si;  $\varepsilon_M$ , Dielectric function of host material (normally: air);  $\varepsilon_{eff}$ , Calculated effective dielectric function;  $P$ , Porosity.

Theory	Formula
Bruggeman	$P \frac{\varepsilon_M - \varepsilon_{eff}}{\varepsilon_M + 2\varepsilon_{eff}} + (1 - P) \frac{\varepsilon - \varepsilon_{eff}}{\varepsilon + 2\varepsilon_{eff}} = 0$
Maxwell Garnett	$\frac{\varepsilon_{eff} - \varepsilon_M}{\varepsilon_{eff} + 2\varepsilon_M} = (1 - P) \frac{\varepsilon - \varepsilon_M}{\varepsilon + 2\varepsilon_M}$
Looyenga	$\varepsilon_{eff}^{1/3} = (1 - P)\varepsilon^{1/3} + P\varepsilon_M^{1/3}$

Table 7. PSi luminescence bands.

Spectral range	Peak wavelength	Label
UV	~ 350 nm	UV band
blue-green	~ 470 nm	Fast (F) band
blue-red	400-800 nm	Slow (S) band
near IR	1100-1500 nm	IR band

Table 8. Some spectral characteristics of the S band.

Property	Typical values	Comments
Peak wavelength	1100-400 nm	At 300 K, depends on porosity
PL External Quantum Efficiency	$\geq 5 \%$	At 300 K, depends on porosity
FWHM	0.3 eV	At 300 K (8 meV in PSi micro-cavities)
PL decay times	$\approx 10 \mu s$	Strongly dependent on wavelengths, temperature and aging condition
Polarisability ratio	$P \leq 0.2$	
Fine structure under resonant excitation	Phonon replica at 56 and 19 meV	Heavily aged PSi, energies consistent with Si phonons

Table 9. Some spectral characteristics of the F band.

Property	Typical values	Comments
Peak wavelength	480 nm	UV excitation at 300K
PL efficiency	$\geq 0.1 \%$	External quantum efficiency UV excitation at 300 K
FWHM	0.4 eV	UV excitation at 300 K
PL decay times	1 ns	Independent on wavelength and excitation conditions

Table 10. Potential application areas of PSi.

application area	role of PS	key property
optoelectronics	LED	efficient electroluminescence
	waveguide	tunability of refractive index
	field emitter	hot carrier emission
	optical memory	non-linear properties
micro-optics	Fabry-Perot filters	refractive index modulation
	photonic band gap structures	regular macropore array
energy conversion	all optical switching	highly non-linear properties
	antireflection coatings	low refractive index
	photo-electrochemical cells	photocorrosion cells
	solar cells	
environmental monitoring	gas sensing	ambient sensitive properties
microelectronics	micro-capacitor	high specific surface area
	insulator layer	high resistance
	low-k material	electrical properties
wafer technology	buffer layer in heteroepitaxy	variable lattice parameter
	SOI wafers	high etch selectivity
micromachining	thick sacrificial layer	highly controllable etching parameters
biotechnology	tissue bonding	tunable chemical reactivity
	biosensors	enzyme immobilization

## Figure captions

Figure 1. Examples of PSi structures: microporous (left), mesoporous (center) and macroporous (right).

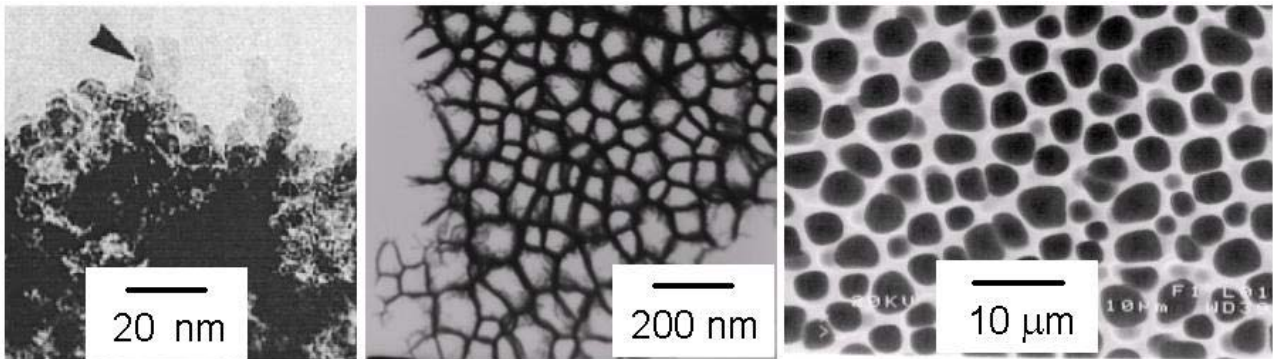
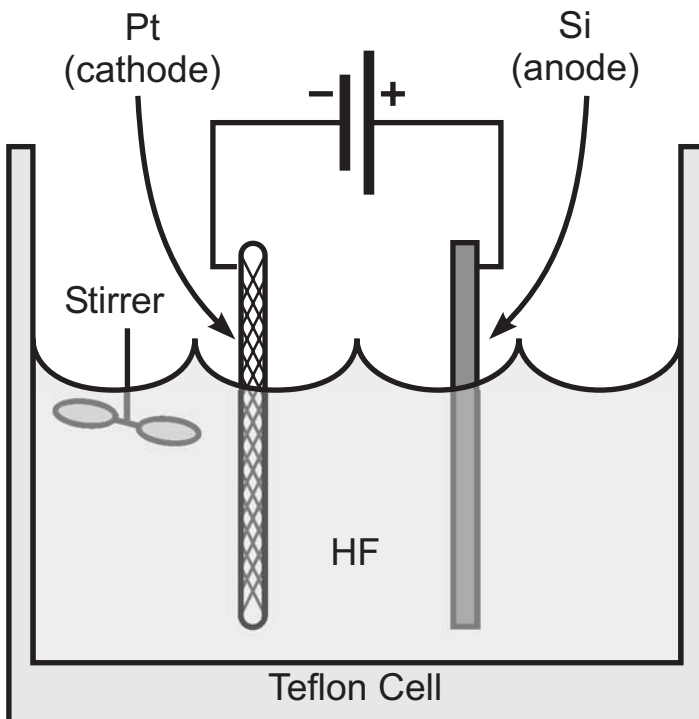


Figure 2. Schematic anodization arrangements: principle (top) and practical examples (A, B and C). Platinum and Teflon are mostly used because of their chemical resistance to HF. In the practical arrangements A B and C, the Si area exposed to the solution — typically about  $1 \text{ cm}^2$ , circular — is well defined by the Teflon cell. Rubber gaskets between Si and Teflon can easily avoid spills. Type A is easier to design, type B is convenient when Si illumination is desirable (for example, for n-type Si, see Section 2), type C does not require electrical contacts on Si. An optional stirrer is sometimes used to improve diffusion of HF during the anodization.



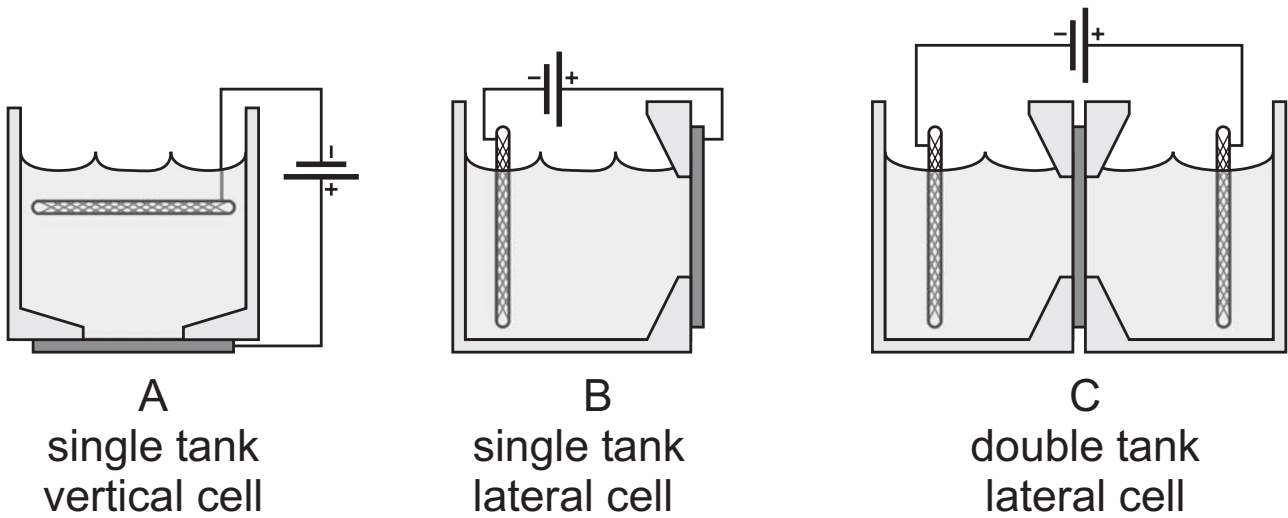


Figure 3. Schematic lithographic procedure resulting in the definition of pore-starting *etchpits*.

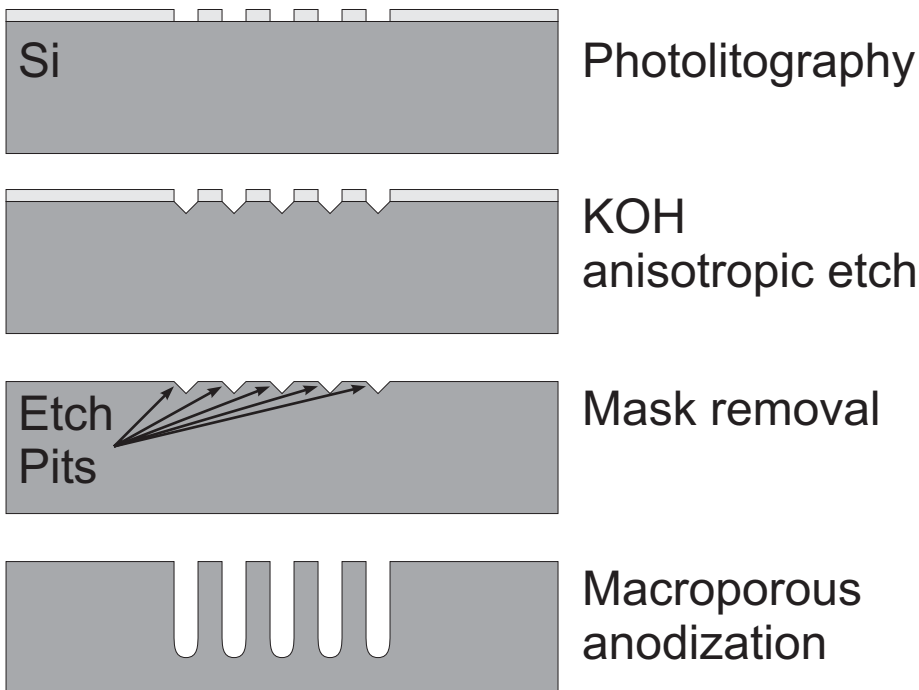


Figure 4. Example of a photonic crystal (cross section and top-view images of the same sample) realized with ordered macroporous PSi in a p-type doped Silicon substrate. This photonic crystal has a photonic band-gap at  $3.5 \mu\text{m}$ .

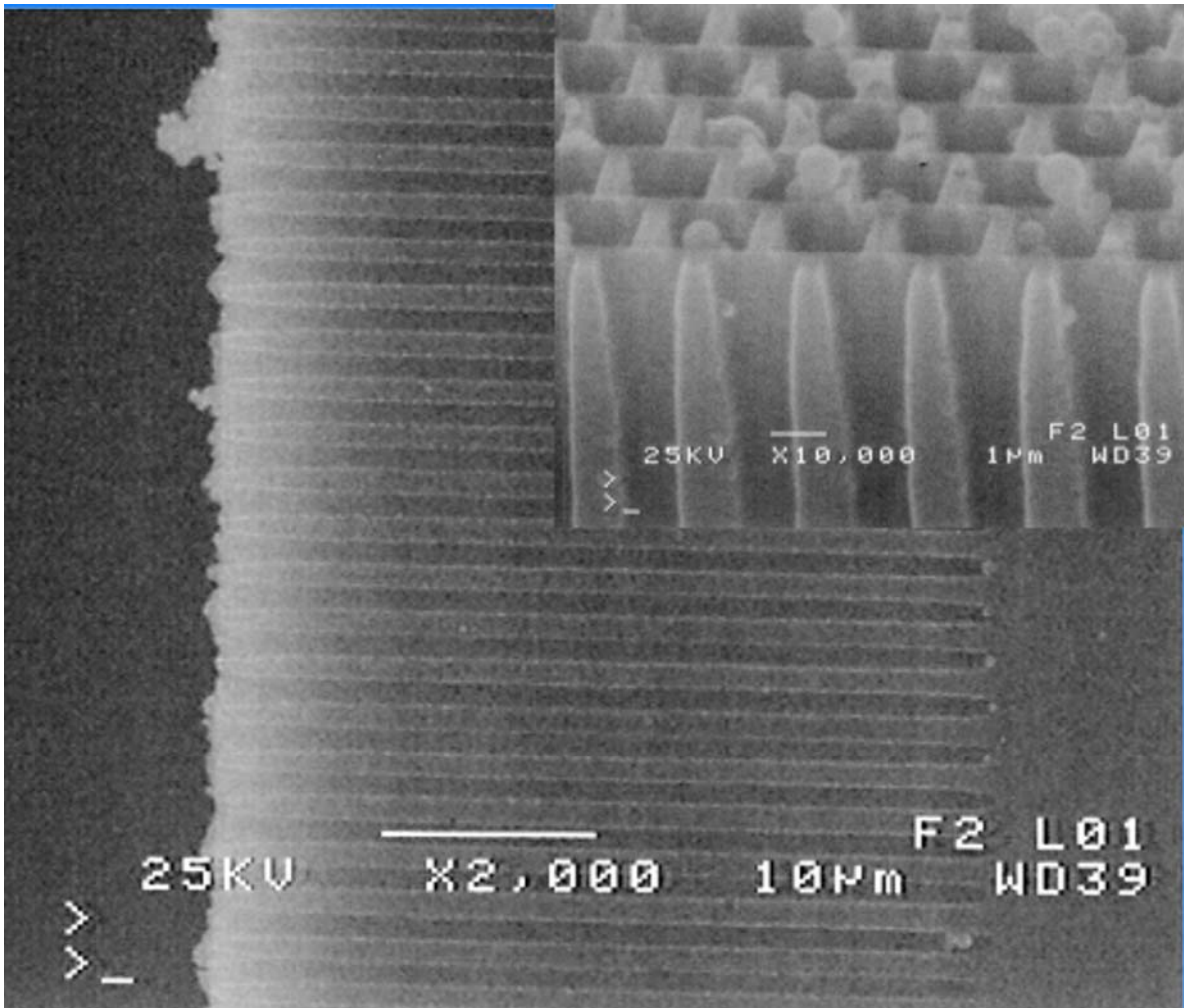


Figure 5. Typical I-V characteristics of an electrochemical cell for PSi fabrication (Figure 2). The hashed region corresponds to the useful regime where PSi can be achieved, assuming the I-V characteristic marked with hollow circles. In the anodic regime, the characteristics of a cell with n-type Si will lay in the region bounded by the characteristic in dark (dashed line) and in full light (hollow circles).

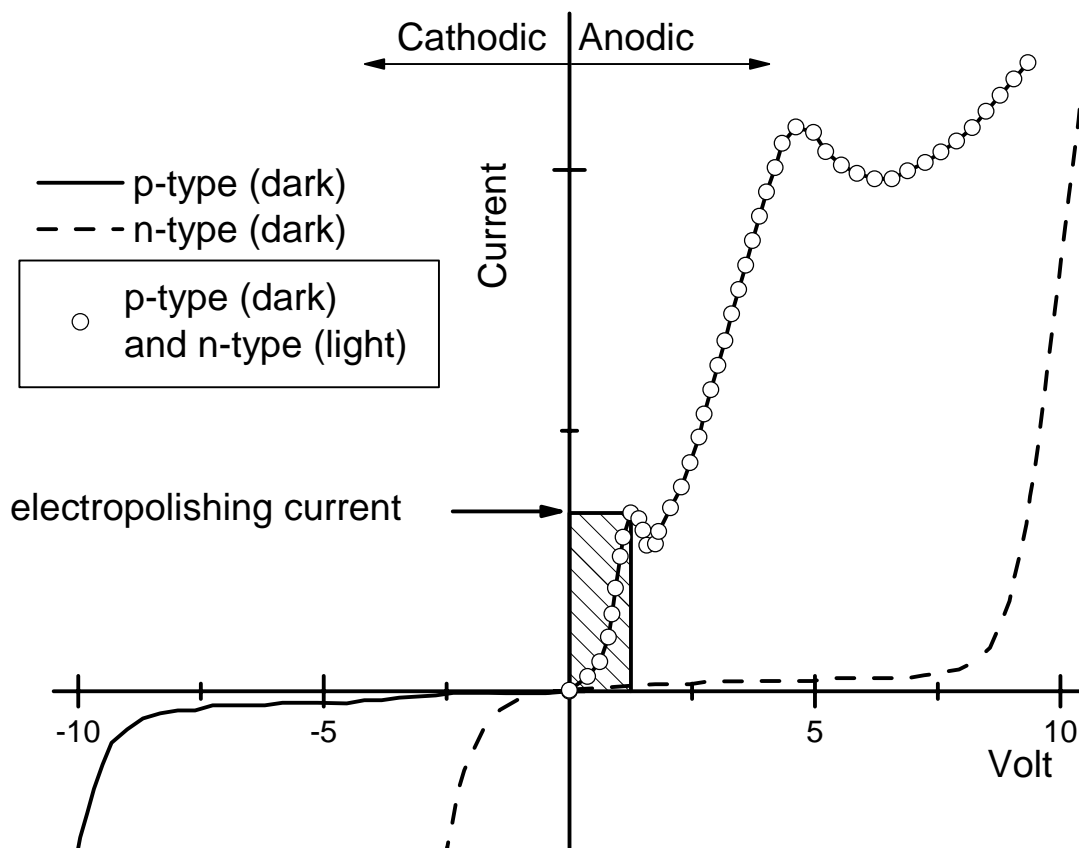


Figure 6. Refractive index as a function of current density and porosity for two different substrate doping levels.

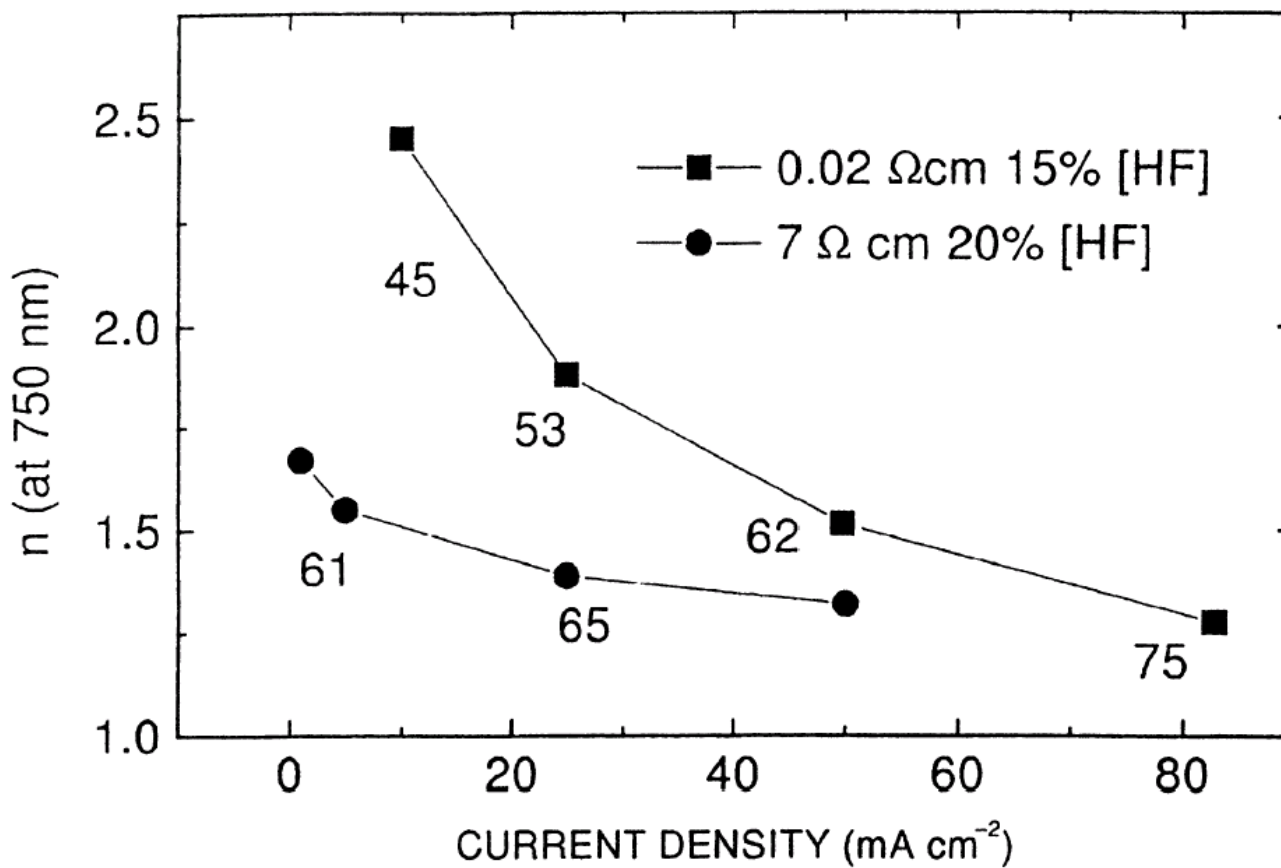


Figure 7. Room temperature photoluminescence spectra for various PSi structures which have been oxidized or implanted with some selected impurities.

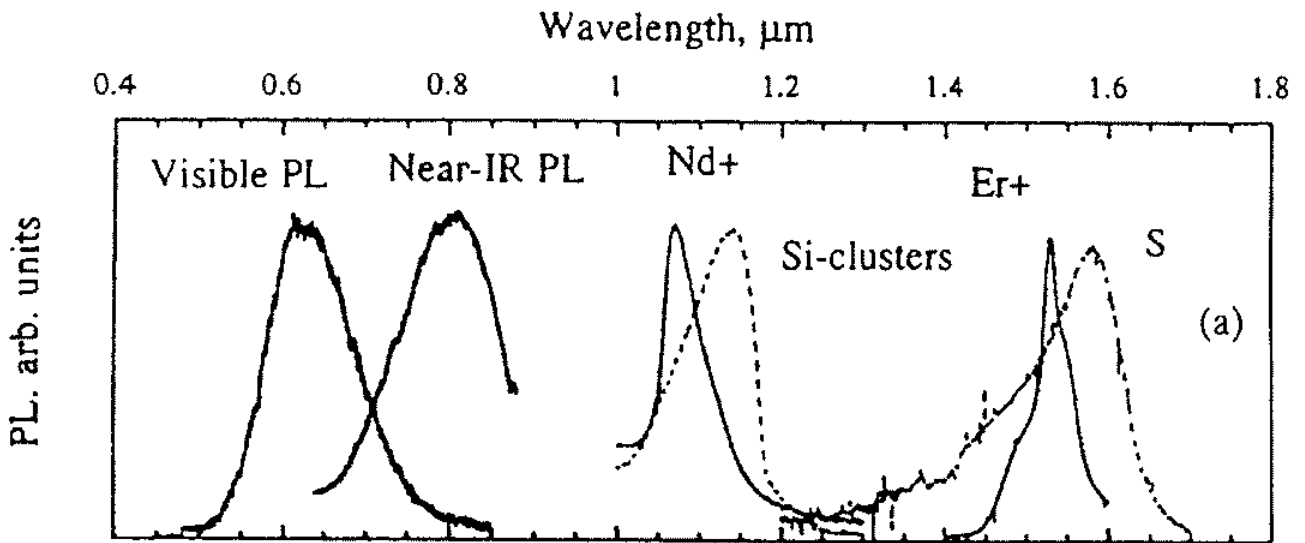


Figure 8. Compilation of optical band gaps of PSi samples obtained from optical absorption (un-filled symbols) and luminescence (filled symbols). The lines represent calculated values with the empirical law reported in the text.

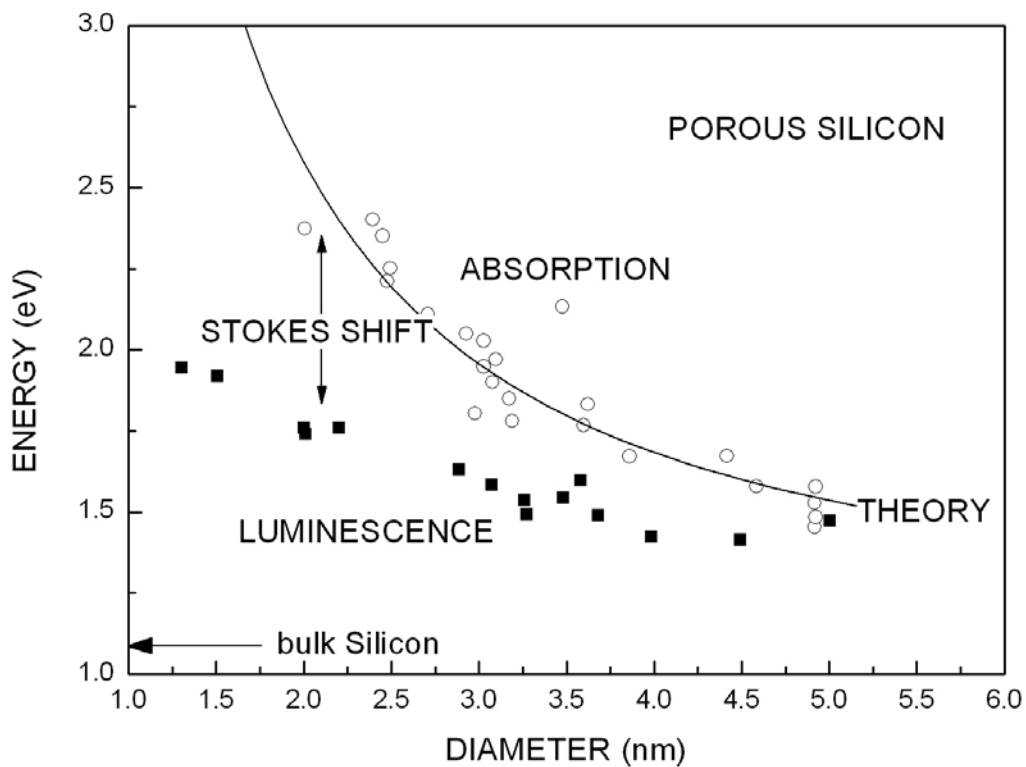


Figure 9. Time evolution of the external quantum efficiency of porous silicon based LEDs for display applications.

### Display Applications

